Available online at www.sciencedirect.com
SCIENCE DIRECT®
Applied Surface Science 252 (2005) 1520–1537
applied surface science
www.elsevier.com/locate/apsusc

Optical multilayer post growth instabilities: Analyses of Gd_2O_3/SiO_2 system in combination with scanning probe force spectroscopy

N.K. Sahoo *, S. Thakur, M. Senthilkumar

Spectroscopy Division, Bhabha Atomic Research Centre, Modular Laboratories, Trombay, Mumbai 400085, India

Received 3 September 2004; received in revised form 24 February 2005; accepted 24 February 2005
Available online 1 June 2005

Abstract

Post growth multilayer instabilities of a certain periodic Gd_2O_3/SiO_2 multilayer systems have been investigated using scanning probe force–distance spectroscopy and optical spectrophotometric techniques. In the present work, we have noticed a strong correlation between the force spectroscopic results and the spectral properties of multilayer thin films, although measurement techniques and operating principles are quite different. From the experimental analysis, it was quite evident that the instability process, which starts during the nucleation and growth stage in thin films, continues to persist at a much longer time scale under post growth conditions. During this study it has been noticed that the elastic properties of the constituent thin films, the layer geometry and the bilayer thickness have strong correlation in trickling the multilayer instabilities. Such aspects also have strong interconnections with the morphological and viscoelastic changes. It is also noticed that most of the instabilities results cannot only be explained through elastic nature of the material alone. Instead, total number of layers, the layer structures, morphological changes, corresponding stiffness and the adhesion properties of the multilayer contribute substantially to these phenomena.
© 2005 Elsevier B.V. All rights reserved.

PACS: 42.79.Wc; 78.66.-w; 78.20.Ci; 61.16.Ch; 51.70.+f; 52.70.Kz

Keywords: Deep UV optical coatings; Multilayer instability; Force–distance spectroscopy; Spectrophotometry

1. Introduction

Stabilities in thin film multilayer and superlattice systems have been very challenging and thought-provoking topics both from the application point of view as well as pedagogical interest [1–4]. A large number of interdependent parameters of the multilayer system always add to the complexity both in understanding and analyzing the instabilities. There are primarily two different kinds of instabilities in multilayer thin films out of which one occurs during the growth stage and the other type evolves under post growth conditions [5,6]. Instability due to mass diffusion process is a very prominent and probable

* Corresponding author. Tel.: +91 22 25593871; fax: +91 22 5505151.
E-mail address: nksahoo@apsara.barc.ernet.in (N.K. Sahoo).

0169-4332/$ – see front matter © 2005 Elsevier B.V. All rights reserved.
doi:10.1016/j.apsusc.2005.02.136

cause mostly during the growth stage of the thin films of having an appreciable nucleation and growth temperature. But in post growth stages, elasticity related effects dominate the instability process. Such process can lead to various stress-relieving outcomes through localized mass transport, grain structure re-ordering and/or morphological changes in thin films and multilayer. Although the characteristics in the instabilities of these two mechanisms may be substantially different, a strong correlation in the initiation as well as evolution of these processes that occur at different time scale can be noticed. Since there exists a wide range of multilayers using different growth mechanisms and geometries, an appropriate technique is required to probe into a particular and desired aspect of such instabilities. The present work is mainly dedicated to study and analyze post growth instabilities of a Gd_2O_3/SiO_2 periodic optical multilayer systems using force–distance spectroscopy of atomic force microscopy and multilayer optical spectrophotometric techniques. Both these pioneering techniques, especially scanning probe force–distance spectroscopy has become a fundamental tool in several fields of research, such as surface science, material engineering, biochemistry and biology [7]. In the present work, we have extended its application to the field of multilayer thin film optical coatings and observed a very useful feed back which helped us to understand the post growth spectral, morphological and elastic instabilities of certain ultraviolet and deep ultraviolet multilayer systems. Although the data presented in this paper belong to a specific multilayer system, these can be conveniently extrapolated for several such systems that use refractory thin film oxides in the multilayer structure. Alternatively, in periodic quarterwave multilayer system the spectral features through spectrophotometric technique can provide voluminous information on the growth as well as post growth instabilities. The spectral bandwidth and reflectance amplitude of quarterwave-thick periodic multilayer system carry a very well defined functional relationship between them [8]. Post growth compositional changes due to environmental effects depict certain predictable functional trend in the reflectance bandwidth as well as spectral peak amplitudes of the multilayers [9]. Effects other than those can be conveniently attributed to the either morphological, viscoelastic changes or stress-driven instabilities [1]. In this situation, scanning probe force–distance spectroscopy has a tremendous potentiality in probing various aspects of the elasticity related effects [10]. In this work, several important parameters of this technique, such as force–distance curve, contact lines, jump-to-contact, jump-off-contact and their slopes (stiffness factors) have been utilized to analyze the elastic and viscoelastic changes of the multilayers associated with the post growth spectral properties changes. It is interesting to note from the experimental results that there exists a strong correlation between the scanning probe force spectroscopic results and the spectrophotometric values, although measurement techniques and operating principles are quite different. A brief overview of these techniques is presented in the subsequent sections. We have also shown in this work that mathematically, elastic and microstructural properties are intimately associated with the physical and geometrical parameters of the multilayer structures. Hence, the prime objective of the present paper is to highlight elastic or viscoelastic changes in multilayer structures that occur during the post growth stages leading to various instabilities pertaining to the morphology as well as optical spectral properties.

2. Elastic properties and multilayer instabilities

The elastic properties of the constituent film materials have great influences on the various aspects of the stability studies relating to the multilayer structures [7,11]. Such aspects include instabilities during growth and post growth stages as well as stress-induced morphological instabilities [3–6,12–16]. There have been quite a few very interesting theoretical papers discussing the various modelling aspects supporting some of the available experimental data [1,2,17,18]. Some research works on multilayer systems also suggested that elastic stresses could induce morphological instabilities leading to formation of islands, nonplaner surfaces or in some cases, the formation of deep, cusplike morphologies [10]. Such morphologies can provide source for the nucleation of stress-relieving dislocations [19–21]. The wavelength of this type of instability is set by the competition between the stabilizing influences of the surface energy and the destabilizing influence of the misfit-induced elastic strain energy. The work of Sridhar et al. has very detailed discussions on these aspects [2]. They have

considered an infinite periodic and symmetric system with the dynamics controlled by interfacial diffusion and focused on the interior layers that are far away from both the surface and the substrate. There is also an extensive theoretical research paper by Huang and Desai on stress-driven instability in growing multilayer films [1]. Their work proposes a recursive procedure and a continuum, dynamic model to describe the morphological evolution in coherent multilayer structures during the epitaxial growth. Some analysis of the studies were also carried out by Shilkrot et al., on the surface diffusion and morphological evolution with respect to the stability of the multilayer systems [3,6,20]. In course of our investigations besides the instabilities, we have also noticed substantial changes in the evolution of morphology and grain structure in various Gd_2O_3/SiO_2 multilayer systems as well. For a system of stacked coherent strained islands (strained/spacer multilayers), in the work of Tersoff et al. [4], each buried island is approximately treated as a point defect, and its contribution to surface strain is determined by using continuum elasticity solutions of Maradudin and Wallis [22]. However, the theoretical analyses of Sridhar et al., have posed a more directional approach in predicting the multilayer stability based on material elastic and interfacial diffusion properties [2]. In the present experimental work, we have considered this elastic approach to explain the origin of instability in the Gd_2O_3/SiO_2 multilayer systems. Subsequently, we have noticed that elastic parameters only cannot explain the post growth instabilities unless one considers the complete multilayer structure including total number of layers. So more theoretical insight to this problem is essential to explain the experimental observations like ours in which layer number dependent instabilities are specifically highlighted in the measurements. However, in this paper, we have confined ourselves to the experimental observations and their analysis only, with the help of the available elastic effect related theoretical modelling proposed by Sridhar et al. [2]. As per this instability theory, when the thicknesses of the constituent layers are comparable, the elastic interactions between them cannot be ignored. The growth related elastic parameter α of a bilayer system is given by [2]:

$$\alpha = \frac{E_A - E_B}{E_A + E_B} \tag{1}$$

where, E_A and E_B are the elastic moduli of the materials A and B, respectively. In our present multilayer systems, gadolinium oxide (Gd_2O_3) with high refractive index is considered as a material A and silicon dioxide (SiO_2) with low values in refractive index as material B. Both these films were deposited at a substrate temperature of 70 °C using reactive electron beam deposition process as described in Section 7. The multilayer elastic growth function 'g' that depends on the bilayer thickness and the above elastic property can be given by [2,23]:

$$g(\alpha, f) = 12\alpha(1-\alpha)\frac{\begin{matrix}[3(1-3f+3f^2)\alpha^2 + \\ 3(1-3f+3f^2)\alpha - 2(1-2f)]\end{matrix}}{\begin{matrix}[1-\alpha(1-2f)]^2 \\ [1-\alpha^2(1-3f+3f^2)]\end{matrix}} \tag{2}$$

where, the thickness fraction $f = h/H$, H is the total bilayer thickness or the overall wavelength of the multilayer, h is the thickness of the component layer A, and the thickness of the associated film material B is $(H - h)$. In this equation, both the types of layers are assumed to be isotropic, linear elastic media with different elastic constants. For a small wavelength limit, the total growth rate is negative provided $g(\alpha, f) \leq 0$ [2]. Consequently for specified relative thickness f, a flat interface in the multilayer system will be stable for a range of α values. It also can be seen that for a volume fraction less than 1/2, the flat interface is unstable for $0 < \alpha < \alpha_c$ and stable for all other α, where α_c is its critical value. For a quarter-wave optical multilayer stack, the physical thickness of the high index layers (A) are less than the low index (B) counterpart, hence the volume fraction for such materials is less than 1/2 as required by the above criterion. Also in our present Gd_2O_3/SiO_2 system the value of $g(\alpha, f)$ is computed to be -0.1840, which very well matches with the requirements of the above equation. The critical elastic control parameter 'α_c' of the bilayers related to f (= h/H) of such a system is given by [2]:

$$\alpha_c = \frac{3(1-3f+3f^2) - [(1-3f+3f^2)(1+5f-5f^2)]^{1/2}}{2(1-2f)(1-3f+3f^2)} \tag{3}$$

such a relationship also focuses on mostly those layers, which are not too close to either the free surface or the substrate. This equation also very interestingly depicted a strong functional behaviour of bilayer thickness or f-factor dependent instabilities. The critical elasticity related parameter α_c has several significances in interpreting multilayer instabilities as it directly deals with interface elastic properties. Obviously, the only deficiency in the above theoretical modelling is the unavailability of functional dependence with respect to the total number of layers in a multilayer structure. In our present experimental studies, it is quite apparent that a combination of elastic properties and total number of layers decide the stability criterion especially in the unstable regions of the multilayer geometry. For periodic quarterwave optical multilayer, the optical thickness, which is a product of the refractive index, and the physical thickness is one fourth of the central wavelength of the devices [8,24], i.e.,

$$n_A(\lambda)h = \frac{\lambda}{4} = n_B(\lambda) \times (H - h) \tag{4}$$

from this expression, the physical thickness values of the associated layers can be easily derived. The dispersive refractive index profiles of Gd_2O_3 and SiO_2 correspond to $n_A(\lambda)$ and $n_B(\lambda)$, respectively. With these index values and the corresponding physical thicknesses, the wavelength dependent elastic control parameters α_c can be easily expressed in terms of the refractive indices of the constituent materials as follows. Using Eq. (4), the f-factors can be expressed as:

$$f = \frac{h}{H} = \frac{n_B(\lambda)}{\{n_A(\lambda) + n_B(\lambda)\}} \tag{5}$$

using this expression and with a little mathematics, the expression for α_c can be given by:

$$\alpha_c = (n_A + n_B) \; 3(n_A^2 + n_B^2 - n_A n_B) \times \left[\frac{-\sqrt{(n_A^2 + n_B^2 - n_A n_B)(n_A^2 + n_B^2 + 7n_A n_B)}}{2(n_A - n_B)(n_A^2 + n_B^2 - n_A n_B)} \right] \tag{6}$$

This is very interesting expression, where the critical elastic parameter α_c is expressed in terms of the film microstructural parameters, which are the refractive indices of the component films. Such an expression also clearly points out the interdependence between the microstructural properties with the physical and spectral parameters in a multilayer thin film system. In the above expression, the wavelength dependence of refractive indices is also reflected in critical elastic coefficient values.

3. Investigating instabilities through force–distance spectroscopy

Atomic force microscopy concern with the fundamental interactions between surfaces extends across physics, chemistry, materials science and a variety of other disciplines [7,25]. Since 1989, this technique has emerged as an essential tool for studying surface interactions by means of force–distance curves, which otherwise known as scanning probe force spectroscopy [25,26]. With force sensitivity of the order of a few piconewtons, AFMs are excellent tools for probing these fundamental force interactions, especially, when adhesion are gaining more and more attention with the development of micro- and nanotechnologies [27]. Due to the reduced masses of moving parts in micromechanical systems the atomic interaction energies invariably dominate the kinetic energies. Atomic Force Microscopes (AFM) allows the measurement of such attractive atomic interaction forces. The application of this technique for tribology is already described in several research papers [7,28].

In a typical force spectroscopy, during the approach of the AFM-tip to a solid sample surface, a ‘‘jump-to-contact’’ instability occurs before zero distance with an undeflected cantilever is reached. During retraction of an AFM-tip pressed against the sample surface it adheres to the surface until the spring force of the cantilever is higher than the attractive interaction force, which undergoes a second instability in terms of ‘‘jump-off-contact’’. These two instabilities, which represent the interaction forces between the sample and the probe strongly, depend on the mechanical, elastic and viscoelastic properties of the interacting materials [7,29–32]. Hence, the dynamical changes in the numerical values of these two instabilities provide voluminous information on the post growth instabilities of a multilayer system. A typical simulated

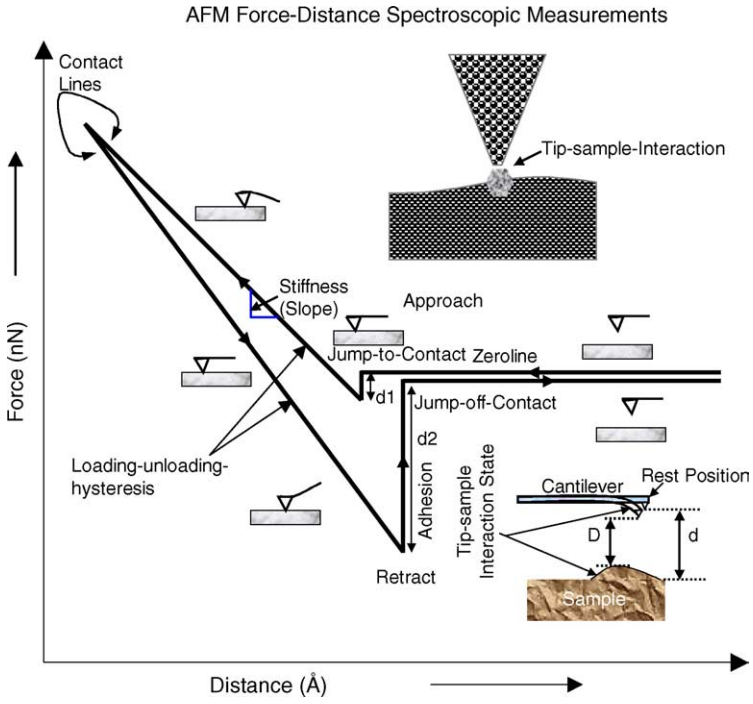

Fig. 1. Explanation of force–distance spectroscopic measurements depicting various important characteristics in the loading and unloading processes.

force–distance curve usually obtained by AFM is depicted in Fig. 1. The force between the AFM-tip and the surface is quantified along the vertical axis, while the horizontal axis shows the tip-surface displacement coordinate. There are several interesting as well very important regions of this force–distance or force–displacement characteristic [7] that has been utilized in this experimental work.

4. The three prime regions of the force–displacement (F–D) curve

Both approach and withdrawal force–displacement curves can be roughly divided in three regions: the contact line, the non-contact region and the zero line [7]. When the sample is pressed against the cantilever the tip is in contact with the sample and $D = 0$, the corresponding lines obtained in the force–displacement curve are called ''contact lines'' as depicted in Fig. 1. Usually, the contact lines provide information on sample stiffness. It is also possible to draw information about the electro-plastic behaviour of the materials from the contact lines of force. The origin of force–displacement curves is usually put at the intersection between the prolongation of the zero line and the contact line of the approach curve. When the sample is elastic in nature, the approach and retraction contact lines usually overlap. Since the most practical samples have mixed behaviour, the loading and the unloading curves seldom overlap as shown in Fig. 1. The difference between the approach and the withdrawal lines is called ''loading–unloading-hysteresis''. Referring to Fig. 1, the distances d1 and d2 are called ''jump-to-contact distance'' and ''jump-off-contact distance''. The adhesion work equals the area between the negative part of the withdrawal curve and the *Z*-axis. The hysteresis of the curve is the difference between the adhesion work and the area between the negative part of the approach curve and the *Z*-axis. The most interesting regions of force–displacement curves are the two non-contact regions, containing the jump-to-contact and the jump-off-contact phenomena. The non-contact region in the approach curves gives information about attractive or repulsive forces before contact. In particular, the maximum value of the

attractive force sampled prior to contact equals the pull-on force, i.e., the product of jump-to-contact and cantilever deflection. The non-contact region in withdrawal curves contains the jump-off-contact. The pull-off force, i.e., the product of jump-off-contact deflection and cantilever force constant equals the adhesion force. In order to relate the tip-sample surface energies and the adhesion force it is necessary to evaluate the deformations and the contact area of the samples. This can be done by means of different theoretical modelling [7].

5. Theories of non-contact region

5.1. Approach curve: attractive forces and jump-to-contact

The jump-into-contact is one of the important quantities that can be measured in a force–distance spectroscopy and it contains very important information on the viscoelastic properties of the interacting force field. As discussed earlier, the discontinuity in this curve occurs when the gradient of the tip-sample force is larger than the elastic constant of the cantilever. The jump-to-contact may be preceded by a region of attractive (Van der Waals or Coulomb force) or repulsive (Van der Waals force in certain liquids, double layer, hydration, and steric) force [7]. The jump-to-contact gives the information on attractive forces between the tip and the sample. The maximum sampled value of the attractive forces equals the jump-to-contact cantilever deflection times the cantilever elastic constant. In order to evaluate such attractive forces, it is necessary to know the force law and the tip shape. The onset of a jump-to-contact is predicted by any theory that takes attractive forces into account (JKR or Maugis) and is also predicted by several numerical calculations [7,33,34]. In AFM measurement the jump-to-contact instability is governed by the stiffness of the cantilever relative to the long-range tip-sample forces. If cantilever elastic constant is bigger than the maximum value of the tip-sample force gradient, then the discontinuity virtually disappear. However, jump-to-contact is always present at an atomic scale, even if the cantilever can be modelled as an infinitely rigid body [7]. In this case, jump-to-contact instability is governed by the stiffness of the tip and the sample materials, related to their cohesive strengths. This phenomenon has been demonstrated by Pethica and Sutton [35] with the help of calculations employing Lennard-Jones potentials and by Landman et al. [36] by use of molecular dynamics (MD) simulations.

In a simplified approach, when the tip is moved towards the surface, the total energy is initially entirely dominated by the elastic energy of the cantilever. Eventually, the attractive force becomes strong enough to impose the global energy minimum. A commonly used form of intermolecular potential V is the Lennard-Jones 6–12 potential given by [37–39],

$$V_{\mathrm{LJ}} = V_0\left[\left(\frac{x_0}{x}\right)^{12} - 2\left(\frac{x_0}{x}\right)^{6}\right] \tag{7}$$

A total potential function, consisting of the sum of the intermolecular and probe elastic function can be given as [39],

$$U_{\mathrm{LJ}}(x) = V(x) + \frac{1}{2}k(x-d)^2 \tag{8}$$

where k, is the spring constant of the cantilever and d is the position of the cantilever. The most eminent feature of the total potential function is the presence of two energy wells with a barrier in between, for a wide range of k and d. Also these two energy function wells (minima) dynamically change during approach and retraction process. During probe approach, the probe well shrinks while the intermolecular well grows, the opposite occurs during the retraction process. When one well dominates the other the cantilever either jump-into or jump-off an equilibrium point, depending upon the potential function's shape and the dynamics. A typical effective interactive potential is depicted in Fig. 2. In this representative calculation the value of the spring constant k is taken as $0.3\,V_0/x_0^2$. It is interesting to note that two instabilities, jump-to-contact and jump-off-contact, depend strongly on the interacting potentials, which in turn depend on the elastic and viscoelastic properties of the sample and the cantilever. There have been several interesting works on these phenomena relating to the SPM force spectroscopy [7].

Pethica and Sutton [35] have shown that in general there exists a minimum separation ($\sim$1–2 Å) below, which the surfaces jump into contact irrespective of

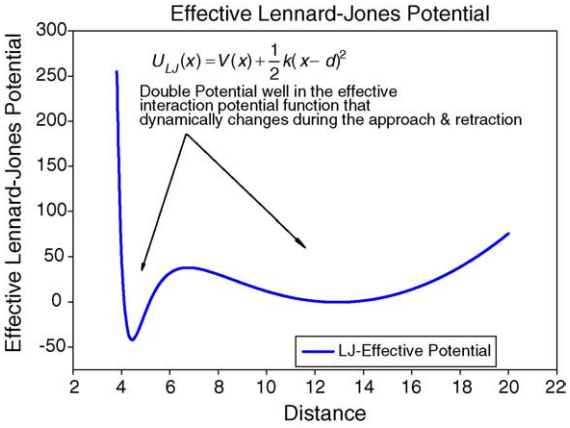

Fig. 2. Lennard-Jones potential computation depicting double potential well that contributes to the jump-in and jump-off-contacts.

the rigidity of the holder. This instability is due to the fact that, at some small enough separation, the gradient of the surface forces exceeds the gradient of the elastic restoring bodies. The instability is irreversible because surface forces have stronger separation dependence than does the elastic restoring force. Lennard-Jones pair potential used by Pethica and Sutton [35] is inapplicable to free surface structures. N-Body potentials of the embedded atom variety are rather much more reliable in such cases. They do not, however, account for long-range attractive forces because they do not incorporate Van der Waals term. Landman et al. [36] verified the onset of jump-to-contact instability by means of MD simulations and compared their results to AFM measurements for a nickel tip interactive with gold substrate. In MD simulations, the tip is modelled as pyramid with an effective curvature of ~30 Å and the sample is made up of 11 layers of 450 atoms per layer. The interatomic interactions governing the energetic and dynamics of the system are modelled by means of embedded-atom method (EAM). In the EAM [40], the dominant contribution to the cohesive energy of the material is viewed as the energy to embed an atom into local electron density provided by other atoms of the system. The presence of the energy barrier prevents the tip-cantilever system. At the distance when the interactive force becomes equal to the cantilever constant, the local minimum due to cantilever elasticity disappears, and the probe abruptly moves to a new position, corresponding to the global minimum, which is ''jump-to-contact'' in this case.

5.2. Withdrawal curve: jump-off-contact and adhesive forces

The second discontinuity or instability of force–displacement curves, the jump-off-contact occurs when, during the withdrawal of sample, the cantilever elastic constant is larger than the gradient of tip-sample adhesive forces [7]. Unlike jump-in, the jump-off-contact is related to tip and sample surface energies via equations that depend on materials dimensions, stiffness and adhesion. The jump-off-contact deflection and jump-off-contact distance are usually greater than jump-to-contact deflection and jump-to-contact distance, respectively. This occurs for several reasons. When the tip is moved toward the surface, the total energy is initially entirely dominated by the elastic energy of the cantilever. Eventually, the attractive force becomes strong enough to impose the global energy minimum. The presence of the energy barrier prevents the tip-cantilever system. At the distance when the net force gradient, $F'_{\mathrm{T}}(D) = k$, the local minimum due to cantilever elasticity disappears, and the probe abruptly moves to a new stable position (jump-off), corresponding to the global minimum. Hence, the nature of these two discontinuities or instabilities if analyzed appropriately can reveal several information on the sample mechanical and viscoelastic properties [41]. The experimental force–distance curves for an unstable 14-layer KrCl(222 nm) laser reflecting multilayer system is presented in Fig. 3(a) and (b) depicting changes during the growth and post growth stages of a time interval of 6 months. It can be seen from these figures that not only the instabilities amplitudes but also their shapes are drastically different at the two different instances.

6. Analysis of instabilities through multilayer spectrophotometry

The spectrophotometry has been a very well known and established technique in probing the spectral response of an optical multilayer device. For a periodic quarterwave-thick multilayer system consisting of an alternative high (n_{H}) and low (n_{L}) refractive

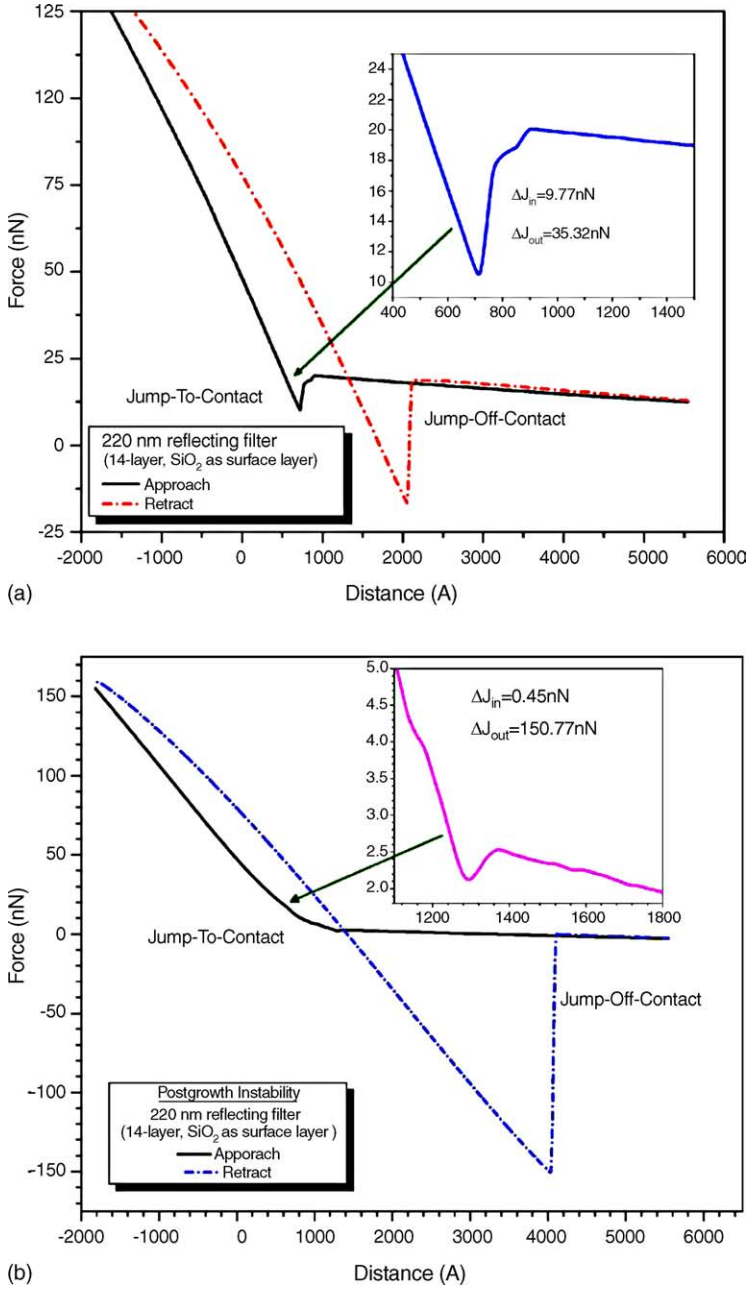

Fig. 3. Force–distance spectra of 14-layer unstable KrCl (248 nm) laser reflecting multilayer measured at two different instances of (a) during growth time and (b) after a period of 6 months.

index, the width of the reflection band (FWHM) in terms of $w = \lambda_o/\lambda$ can be given by the formula [24],

$$\mathrm{FWHM} = 2\,\Delta w = \frac{4}{\Pi}\sin^{-1}\left(\frac{n_H - n_L}{n_H - n_L}\right) \tag{9}$$

where n_H, n_L are the refractive indices of the high and low index layers, respectively. Also λ_o and λ are the central and the scanning wavelengths, respectively.

Similarly, the amplitude of such a multilayer system is given by:

$$R_{MAX} = \left(\frac{1 - (n_H/n_L)^{2p}(n_H^2/n_S)}{1 + (n_H/n_L)^{2p}(n_H^2/n_S)}\right)^2 \tag{10}$$

where $(2p + 1)$ is the number of layers in the multilayer and n_S is refractive index of the substrate. Similar expressions also can be derives for even number of layers. It can be seen from both these equations that values for FWHM and R_{MAX} will have similar functional trend when the refractive index values for the two materials are either increased or decreased. That means, due to the environmental effect when the refractive indices of the two material increases both R_{MAX} and FWHM should also increase. Opposite is the case when the index values should decrease. A typical simulation to the environmental related index changes on the spectral properties of a 13-layer multilayer system is presented in Fig. 4. Effects other than the compositional changes due to the environmental effect may depict different kinds of functional trend in the R_{MAX} and FWHM values. To mention a few of such instabilities are stress-driven, morphological, interfacial/interdiffusion related instabilities [2].

Mostly compositional instability in oxide multilayers is associated with penetration of ambient moisture into the structure and alters the refractive index (usually increases) of the individual layer system. Such a change that affects the ratios of refractive indices has a very well defined impact on the spectral properties that include the change in bandwidth and the amplitude of the reflectance characteristics of the quarterwave multilayers. It can be noticed from the above equations that amplitude and bandwidths are intimately interdependent and strongly associated with the index ratios. When the index ratio goes low, values of both the spectral parameters also decrease and reverse is the case when the index ratio goes high. Broadly speaking, under compositional changes, values for both the bandwidth

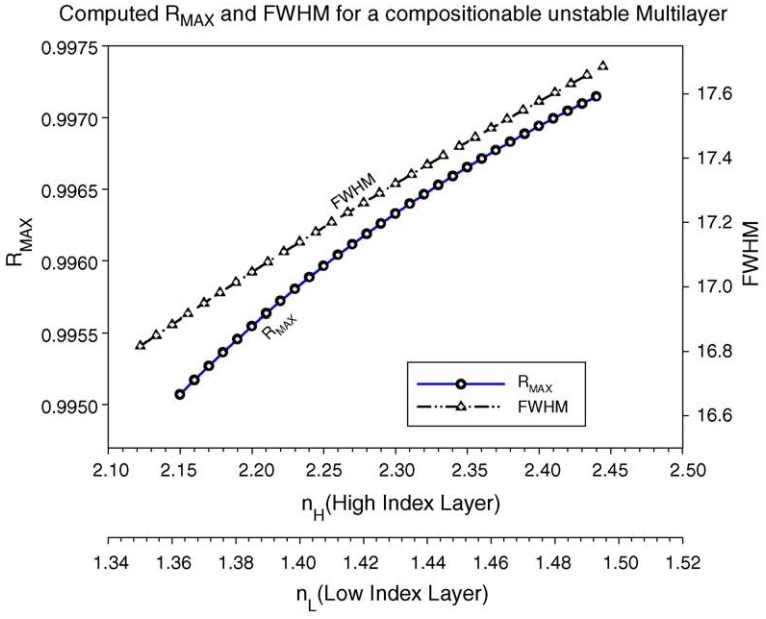

Fig. 4. Computed reflectance maximum (R_{MAX}) and the FWHM of a 13-layer compositionally unstable multilayer varying both high and low refractive indices of the component layers.

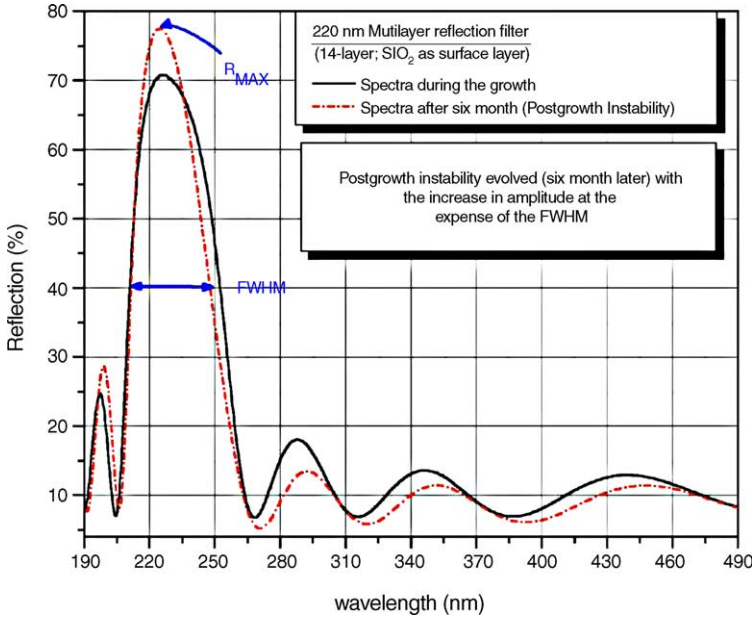

Fig. 5. Spectral R_{MAX} and FWHM measurements of the unstable 14-layer multilayer through spectrophotometry. The post growth measurements were carried out after an interval of 6 months.

and the amplitude should simultaneously increase. It is interesting to note that under our present investigations, different types of spectral variations were noticed in most of the multilayer systems, which include the increase in the reflectance amplitude with the decrease of FWHM, etc. Such anomalous spectral properties may be attributed to the predominantly morphological, elastic or stress-driven instabilities. The experimental spectral measurement of a most unstable 14-layer multilayer is depicted in Fig. 5. This figure shows both the growth and post growth (6-month later) related spectral reflectance measurements results. As it can be seen, the post growth instabilities have shown an increase in the reflectance amplitude of the stop band and a decrease in the value of its spectral width (FWHM). Such a change cannot be explained through compositional changes as described earlier. The topographic changes of this unstable multilayer system is depicted in Fig. 6(a) and (b). It can be observed in this figure that the topography has been substantially changes with respect to the grain sizes as well as RMS roughness values. The viscoelastic changes of these multilayers acquired through force modulation technique are

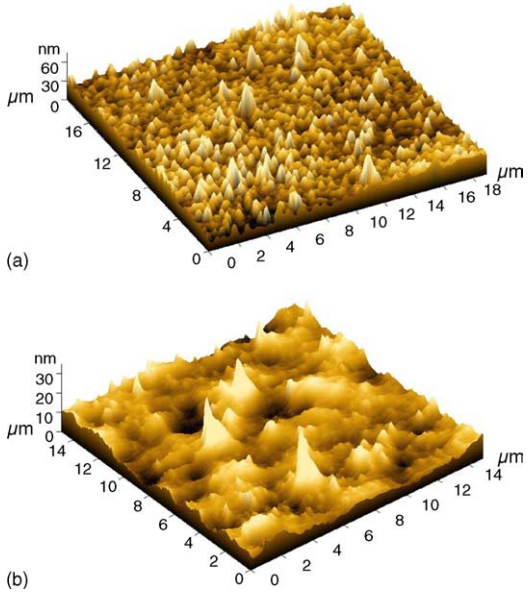

Fig. 6. (a) Growth and (b) post growth topographic changes of the 14-layer unstable reflecting multilayer depicting notable changes in the morphology.

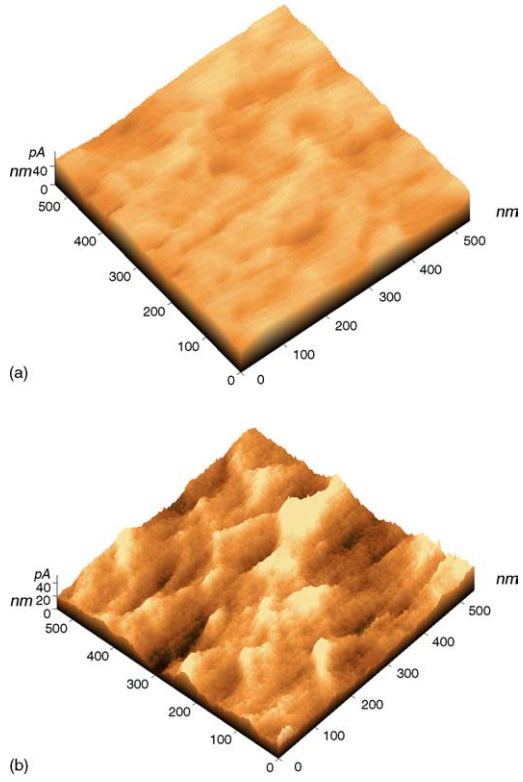

Fig. 7. (a) Growth and (b) post growth viscoelastic changes in the force modulation measurements of the 14-layer unstable reflecting multilayer depicting notable changes in the stiffness distributions.

depicted in Fig. 7(a) and (b). There are substantial changes in the stiffness distribution leading to a completely different viscoelastic image as shown in Fig. 7(b). Such changes have pointed out to strong correlations amongst the spectral, morphological and elastic instabilities as discussed by several other experimental works.

These aspects also were reflected in the topographic and viscoelastic properties as measured through the force–distance spectroscopy. The values of jump-to-contact and jump-off-contacts very interestingly follow a systematic as well as symmetric functional trend with respect to the spectral changes. In the present paper, we have noticed a strong correlation between the scanning force spectroscopic results and the spectrophotometric values, although measurement, operating principles and mechanisms are quite different. Following sections discuss some of our experimental results and their analyses.

7. Experimental

Several multilayer filters have been designed and developed for various excimer laser wavelengths using Gd_2O_3 as high index and SiO_2 as low index layers [42]. Such reflecting filters include (i) 41-layer reflector for 193 nm ArF Laser, (ii) 31 and 14-layer reflection filter for 222 nm KrCl laser, (iii) 25-layer reflector for 248 nm KrF laser and (iv) 21-layer multilayer for 355 nm XeF laser. Such wide varieties of designs were tried out in order to study the systematic changes in the spectral and viscoelastic instabilities of these all dielectric multilayer reflectors over the time.

Under the present investigation, we have carried out some systematic experiments and analysis on post growth instabilities of these multilayers using a multimode scanning probe and spectrophotometric techniques. The samples were deposited in a fully automatic thin film vacuum system ''VERA-902'' by adopting the reactive electron beam deposition technique. The depositions of the films were carried out using an 8 kW VTD electron beam gun with sweep and automatic emission controls. The film materials for SiO_2 and Gd_2O_3 were chosen from Cerac's batch number ''S-1060'' (purity 99.99%) and ''G-1076'' (purity 99.9%), respectively. The substrate temperature was maintained at 70 °C for both the films. The total pressure inside the chamber during the deposition process was maintained at 1×10^{-4} mbar through MKS mass flow controllers. The constituents of the gases present during the deposition were analyzed by a residual gas analyzer (RGA) model; Pffeier's Prisma-200. The film thicknesses were monitored both using the Leybold's OMS-2000 OTM (optical thickness monitor) as well as Inficon's XTC/2 QCM (quartz crystal monitors). The typical rate of depositions was maintained at 1 nm/s for most of the films. The entire deposition process parameters, such as substrate temperature, rate of deposition, total reacting gas pressure were monitored and controlled by a Siemen's industrial programmable logic controller with an appropriate front-end software. The film thicknesses were kept constant at quarterwave thickness at the

respective laser wavelength. For 248 nm (KrF laser) wavelength this amounts to be approximately 31 nm for Gd_2O_3 and 42 nm for SiO_2 layers in terms of their physical thicknesses.

For AFM characterization, NT-MDT's solver P-47H multimode ambient-based scanning probe system has been utilized. The cantilever used was a Si_3N_4 with typical spring constant of 0.6 N/m and resonant frequency of 75 kHz. We have adopted the contact mode operation without any image filtering technique for the topographic measurements. For Fourier analysis, the built-in FFT module of the control software "NOVA-SPM" was employed to generate the mappings. In order to have the consistency in the experimental results, the same cantilever was used for all the force–distance spectroscopy measurements. All the multilayers were spectrally measured for their reflectance as well as transmittance characteristics using Shimadzu UV3101PC spectrophotometer system. Spectral characteristics were recorded initially just after the development and subsequently after 6 months in order to observe the spectral changes/instabilities with respect to aging under normal ambient conditions. It was noticed that the multilayers terminated with low index SiO_2 layer have shown relatively more temporal degradation in spectral characteristics than the structure ended with Gd_2O_3 layers.

8. Results and discussions

Fig. 8 depicts the changes of spectral parameter with respect to change in jump-to-contact forces in several periodic multilayers. The two curves represent the changes in the bandwidth (FWHM) and peak amplitudes, respectively. It is interesting to note that for most of our multilayers these two spectral parameters have shown the changes in the opposite direction with different amount in their values. Such changes as discussed earlier, points out instability other than the environmental related compositional type. The data values in Fig. 8 are fitted with the appropriate polynomials in order to present smooth functional trend. The highest instability values were depicted for a 14-layer KrCl (222 nm) reflecting multiplayer, which has bilayer thickness of 64.77 nm ($f = 0.439$). The 41-layer ArF (193 nm) reflecting filter with a bilayer thickness of 54.26 nm ($f = 0.428$) also showed some amount of instability. The lower values were recorded for 24-layer as well as 25-layer reflecting multilayers designed for KrF (248 nm) laser wavelength with a

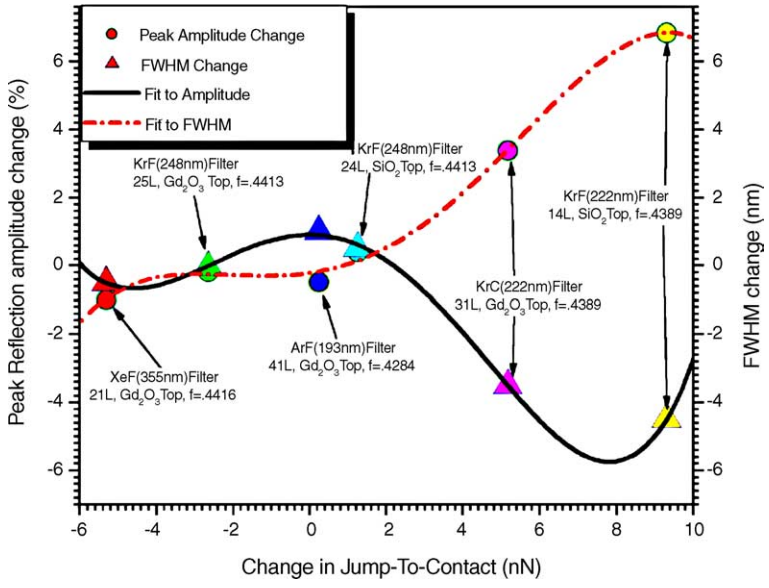

Fig. 8. Plot of spectral parameter changes with respect to changes in jump-to-contact parameters of various Gd_2O_3/SiO_2 multilayers carrying various *f*-factors.

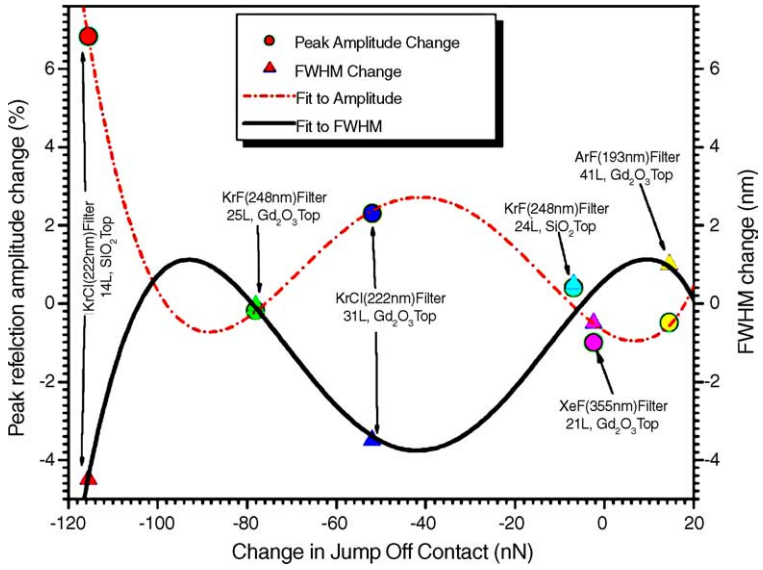

Fig. 9. Plot of spectral parameter changes with respect to changes in jump-off-contact parameters of various Gd_2O_3/SiO_2 multilayers.

bilayer thickness of 73.48 nm ($f = 0.441$). The results for this wavelength have demonstrated maximum stability. Similarly, the 21-layer multilayer for XeF (355 nm) laser with bilayer thickness of 108.64 nm ($f = .447$) has shown reasonably good stability. Overall, the multilayers with smaller positive or negative changes in the jump-to-contact forces have depicted better stabilities. Fig. 9 depicted the spectral parameter changes with respect to the changes in the jump-off-contact forces. In this case also the same 14-layer (KrCl laser reflector) multilayer with the bilayer thickness of 64.6 nm depicted both the highest spectral instability as well as larger viscoelastic changes. The better spectrally stable 248 nm multilayers (bilayer thickness of 73.48 nm) showed a negligible as well as higher negative values in the change of jump-off-contact force variations depending on the multilayer geometry and the surface layer. The spectral data versus jump-off-contact values were fitted with a polynomial function to represent a smooth functional dependence. Both the curves showed systematic periodic variations where the stable multilayers are found to be positioned at or close to the node-like points. It is interesting to note from both these experimental results that the multilayer reflectors carrying bilayer thickness below a certain value have shown maximum instability. That is, multilayers meant for ArF laser (bilayer thickness 54.26 nm, $f = 0.428$) and KrCl laser (bilayer thickness 64.77 nm, $f = 0.439$) has shown higher degrees of instabilities. Such observations have found to have close relationships with the elastic properties and f-factors of the component film material as discussed by Sridhar et al. We have computed the elastic coefficient α for the Gd_2O_3/SiO_2 bilayer system by considering some published elastic coefficients for these materials for our present substrate temperatures [43]. By taking elastic moduli of Gd_2O_3 and SiO_2 as 140.6 and 73.61 GPa, respectively for the substrate temperature conditions of 70 °C, the α value can be computed as 0.312 using Eq. (1). The critical value α_c of different multilayer system have been evaluated by using appropriate bilayer thicknesses (f-factors) from the refractive index values of the film material involved in the structure. The dispersive refractive index values for Gd_2O_3 and SiO_2 are depicted in Fig. 10. We have plotted the critical α_c versus wavelength of Gd_2O_3/SiO_2 system and noticed a dispersive behaviour as it can be seen from Fig. 11. The computed α value (= 0.312) has been plotted as a straight line in this graph. It is interesting to see that the multilayers meant for ArF laser (193 nm) and KrCl laser (222 nm) wavelength have critical α_c values greater than the α value (=0.312) for the quarterwave Gd_2O_3/SiO_2 multilayer systems. In spectral measurements also multilayers belong to these wavelength have

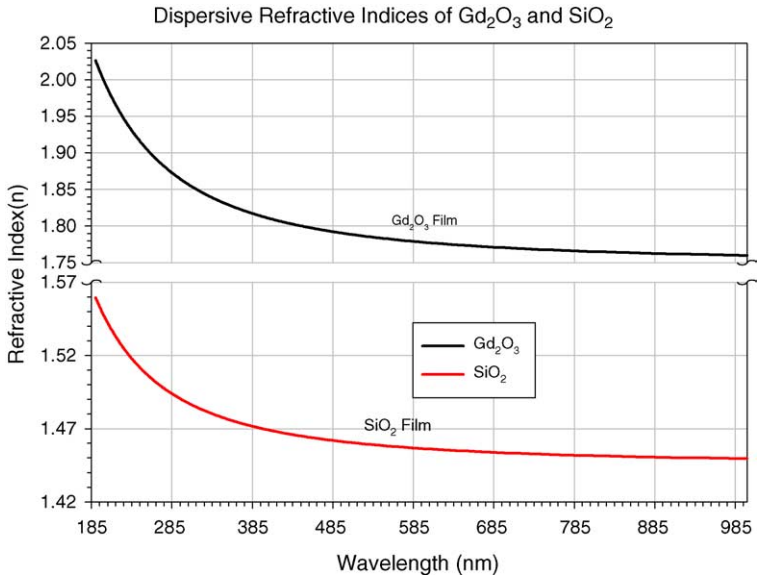

Fig. 10. Experimental spectral refractive profiles of Gd_2O_3 (n_H) and SiO_2 (n_L) optical films deposited through reactive electron beam deposition technique.

depicted most instabilities. However, one of the contrasts that is observed in this analysis that the multilayers belonging to ArF laser (193 nm) should have had instability factors higher than the KrCl laser (222 nm) mirrors, because of relatively more deviations in the elastic coefficients. Whereas, the experimental spectral measurements shows less instabilities in ArF laser reflectors than the KrCl laser multilayers and this

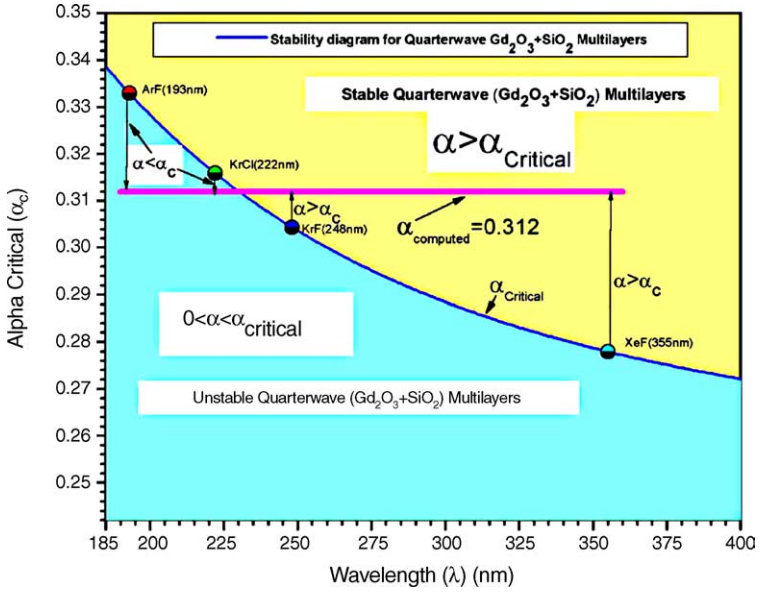

Fig. 11. Plot of computed values of α and the experimental values of α_c for various Gd_2O_3/SiO_2 multilayers. This plot distinctly depicts the bilayer thickness dependent elastic instabilities only in certain multilayer systems.

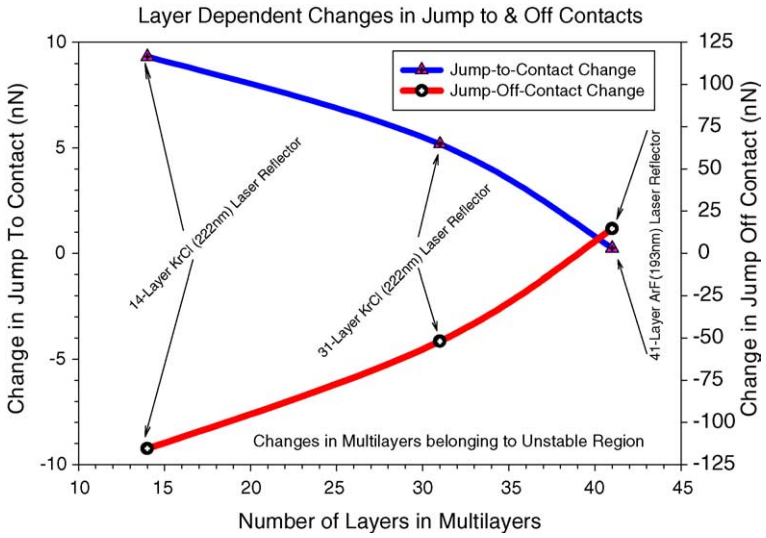

Fig. 12. Layer number dependent changes in jump-to-contact and jump-off-contact values for the unstable multilayers.

may be now accountable to the total number of layers in the structures. In order to investigate this aspect further, we have presented the jump-to-contact and jump-off-contact values for the instable multilayers in Fig. 12. It can be noticed from this plot that both the viscoelasticity related jump-to-contact and jump-off-contact values have approach to a minimum absolute value for the multilayers with certain layer numbers in the geometry. The similar information can also be seen from the graphs in Fig. 13 where spectral data are presented with respect to the layer numbers. It is noticed from this presentation that for elastically unstable multilayer system, the spectral instability can be reduced appreciably by choosing appropriate number

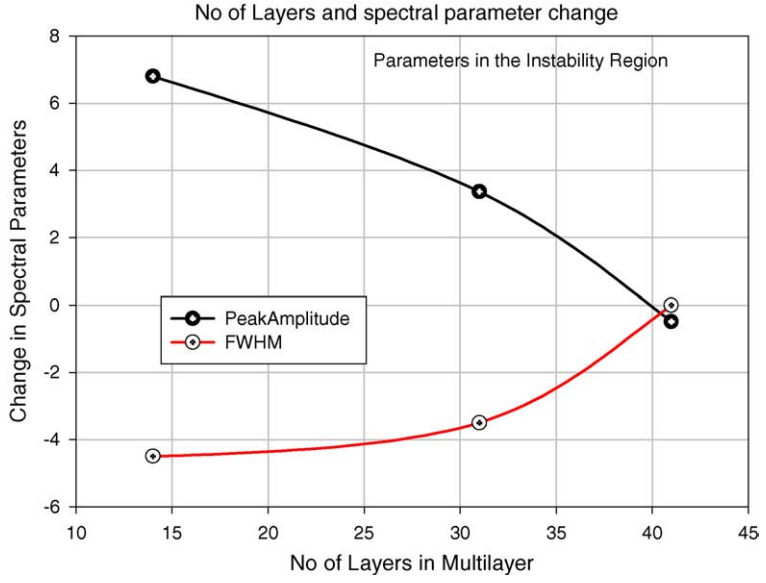

Fig. 13. Layer number dependent spectral parameter changes for unstable multilayers.

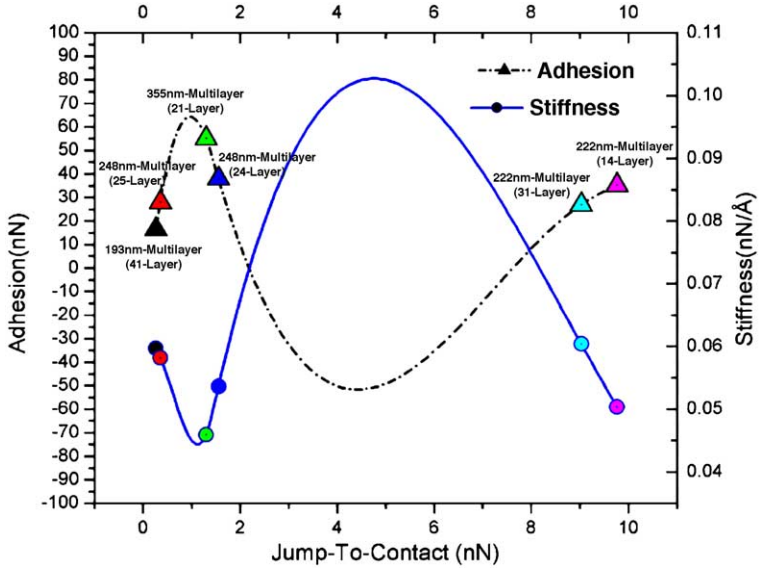

Fig. 14. Changes in the stiffness and adhesion values with respect to jump-to-contact values for various stable and unstable multilayers.

of layers in the system. Another interesting information on the adhesion and stiffness measurement results on various multilayer systems are presented in Fig. 14. In this figure, it is interesting to note that the initial values (i.e., growth stage values) in adhesion and stiffness have depicted opposite trends for various multilayers, which means that the multilayers with better adhesions will have lower stiffness values and the vice versa. But for unstable multilayers, the jump-to-contact is found to be a very sensitive parameter to explain the present instability. In our case both 14-layer as well as 31-layer 222 nm (KrCl laser) reflecting multilayers depicted

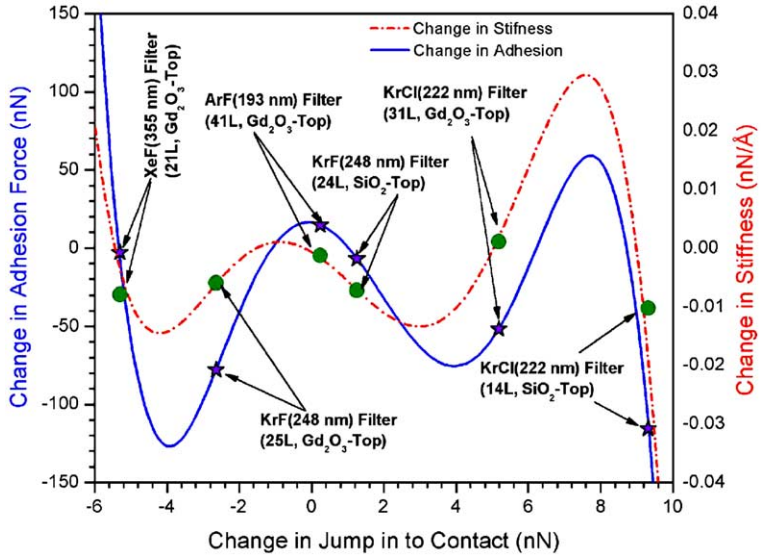

Fig. 15. Plot of the change in adhesion and the stiffness values for various multilayers depicting close relationship between them during the evolution of the instabilities.

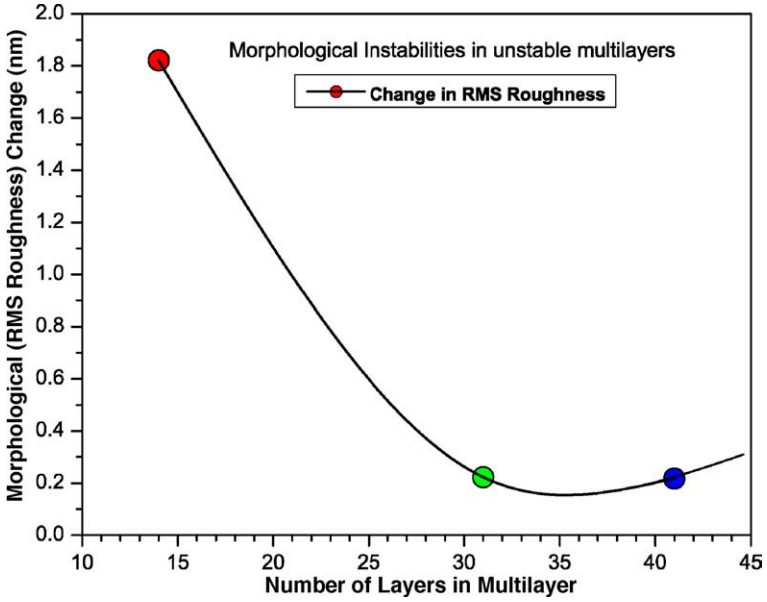

Fig. 16. Depiction of morphological instability in unstable multilayers. It can be seen that the changes in RMS roughness values for the unstable multilayers substantially decrease as the number of layers in a multilayer increased.

high jump-to-contact values. The relationship between stiffness and adhesion force for all of our multilayers is depicted in Fig. 15. It is noticed here that change in adhesion and the stiffness factors (instabilities) both follow a very similar characteristics with respect to various multilayer layer structures and geometry. This indicates that stiffness and adhesion evolutions at a longer time scale (post growth stages) can demonstrate a similar type of trends. The results on the morphological changes with respect to number of layers in the unstable multilayers are depicted in Fig. 16. It can be seen from this plot that the morphological changes are minimum for the unstable multilayers with certain optimum number of layers. Beyond the optimum value the morphological instability depicts an increasing trend. These results also hinted towards the close association of morphological instability with the elastic and spectral instabilities in the multilayer systems. So for elastically unstable periodic bilayer systems, it is always possible to achieve a better stability factors by appropriately choosing the total number of layers in the multilayer geometry. The stability factors in such multilayers improve most likely due to appropriate values in the stiffness and adhesion properties of the component layer systems.

9. Conclusions

The present work deals with the experimental investigations and analysis of the post growth instabilities aspects of Gd_2O_3/SiO_2 multilayer system based on scanning probe force spectroscopy and optical spectrophotometric results. During analysis a very good close correlation were noticed between the results of these techniques. It was interesting to note that the most important phenomena, jump-to-contact and jump-off-contact, of the force–distance spectroscopy which deals with elastic properties of materials have agreed very well with spectral measurements using the spectrophotometric techniques. It is a very good example of coexistence of diversified analysis approaches in probing and explaining instabilities in precision multilayer systems. The most elastic based theories that are applicable for the growth stage of the thin films can be conveniently applied to a much longer time scale of post growth instabilities. Besides the elastic properties of the component materials, the layer geometry, structures and the total number of layers have strong impacts on the multilayer instabilities. Some of the existing theoretically approaches have to be appropriately extended in

accommodating more number of multilayer parameters to explain various experimental results.

References

[1] Z.-F. Huang, R.C. Desai, Phys. Rev. B 67 (2003) 075416.
[2] N. Sridhar, J.M. Rickman, D.J. Srolovitz, J. Appl. Phys. 82 (1997) 4852.
[3] L.E. Shilkrot, D.J. Srolovitz, J. Tersoff, Appl. Phys. Lett. 77 (2000) 304.
[4] J. Tersoff, C. Teichert, M.G. Lagally, Phys. Rev. Lett. 76 (1996) 1675.
[5] S.F. Pellicori, E. Colton, Thin Solid Films 209 (1992) 109.
[6] L.E. Shilkrot, D.J. Srolovitz, J. Tersoff, Phys. Rev. B 62 (2000) 8397.
[7] B. Cappella, G. Dietler, Surf. Sci. Rep. 34 (1999) 1.
[8] Sh. Furman, A.V. Tikhonravov, Basics of Optics of multilayer systems, Frontier editions, Gif-sur Yvette, 1992.
[9] S.F. Pellicori, H.L. Hettich, Appl. Opt. 27 (1988) 3061.
[10] W.H. Yang, D.J. Srolovitz, J. Mech. Phys. Solids 42 (1994) 1551.
[11] J. Mirecki-Millunchick, R.D. Twesten, D.M. Follstaedt, S.R. Lee, E.D. Jones, Y. Zhang, S.P. Ahrenkiel, A. Mascarenhas, Appl. Phys. Lett. 70 (1997) 1402.
[12] K.C. Hsieh, J.N. Baillargeon, K.Y. Chang, Appl. Phys. Lett. 57 (1992) 2244.
[13] K.Y. Cheng, K.C. Hsieh, J.N. Baillargeon, Appl. Phys. Lett. 60 (1992) 2892.
[14] S.T. Chou, K.Y. Cheng, L.J. Chou, K.C. Hsieh, J. Appl. Phys. 78 (1995) 6270.
[15] N.Y. Jin-Phillipp, F. Phillipp, T. Marschner, W. Stolz, J. Mater. Sci. Mater. Electron 8 (1997) 289.
[16] D. Josell, W.C. Carter, J.E. Bonevich, Nanostruct. Mater. 12 (1999) 387.
[17] A. Ponchet, A. Rocher, A. Ougazzaden, A. Mircea, J. Appl. Phys. 75 (1994) 7881.
[18] R.D. Twesten, D.M. Follstaedt, S.R. Lee, E.D. Jones, J.L. Reno, J. Mirecki-Millunchick, A.G. Norman, S.P. Ahrenkiel, A. Mascarenhas, Phys. Rev. B 60 (1999) 13619.
[19] Z.F. Huang, R.C. Desai, Phys. Rev. B 65 (2002) 205419.
[20] J.D. Eshelby, Proc. R. Soc. London Ser. A 241 (1957) 376.
[21] D.E. Jesson, S.J. Pennycook, J.M. Baribeau, D.C. Houghton, Phys. Rev. Lett. 71 (1993) 1744.
[22] A.A. Maradudin, R.F. Wallis, Surf. Sci. 91 (1980) 423.
[23] N. Sridhar, J.M. Rickman, D.J. Srolovitz, Acta Mater. 45 (1997) 2715.
[24] H.A. Macleod, Thin film optical filters, second ed., IOP Publishing, Bristal, Philadelphia, 2001, Chapter 5, p. 179.
[25] G. Binnig, C.E. Quate, Ch. Gerber, Phys. Rev. Lett. 56 (1986) 930.
[26] E. Meyer, H. Heinzelmann, P. Grtitter, Th. Jung, Th. Weisskop, H. Hidber, R. Lapka, H. Rudin, J. Gtintherodt, J. Microscop. 152 (1988) 269.
[27] H.P. Lang, M. Hegner, E. Meyer, Ch. Gerber, Nanotechnology 13 (2002) R29.
[28] E. Meyer, R. Lüthi, L. Howald, W. Gutmannsbauer, H. Haefke, H. Güntherodt, Nanotechnology 7 (1996) 340.
[29] U. Landman, W.D. Luedtke, J. Vac. Sci. Technol. B 9 (1991) 414.
[30] D. Ricci, M. Grattarola, J. Microscop. 176 (1994) 254.
[31] D. DeVecchio, B. Bhushan, Rev. Sci. Instrum. 68 (1997) 4498.
[32] D.H. Gracias, G.A. Somoraj, Macromolecules 31 (1998) 1269.
[33] P. Attard, J.L. Parker, Phys. Rev. A 46 (1992) 7959.
[34] J.A. Greenwood, Proc. R. Soc. London A 453 (1997) 1277.
[35] J.P. Pethica, A.P. Sutton, J. Vac. Sci. Technol. A 6 (1988) 2400.
[36] U. Landman, W.D. Luedtke, N.A. Burnham, R.J. Colton, Science 248 (1990) 454.
[37] W. Chang, J. Hsu, T. Lai, J. Phys. D Appl. Phys. 37 (2004) 1123.
[38] H. Hölscher, U.D. Schwarz, R. Wiesendanger, Appl. Surf. Sci. 140 (1999) 344.
[39] B.E. Shapiro, H. Qian, J. Theoret. Biol. 194 (1998) 551.
[40] S.M. Foiles, M.I. Baskes, M.S. Daw, Phys. Rev. B 33 (1986) 7893.
[41] R.M. Lynden-Bell, Science 263 (1994) 1704.
[42] N.K. Sahoo, S. Thakur, M. Senthilkumar, D. Bhattacharyya, N.C. Das, Thin Solid Films 440 (2003) 155.
[43] R.G. Munro, Elastic Moduli Data for Polycrystalline Ceramics, NISTIR, Gaithersburg, Maryland 20899, 2002, p. 6853.